# DESIGN AND FABRICATION OF INPUT RF COUPLER WINDOWS FOR THE SNS\*

Quan-Sheng Shu, Joe Susta, Guangfeng Cheng AMAC International Inc, Newport News, VA 23606 (USA) Steven Einarson, Todd. A. Treado, William C. Guss, and Michael Tracy Communication and Power Industries Inc. (CPI), Beverly, MA 01915-5595 (USA)

#### Abstract

The RF coupler was designed by AMAC to meet the specification requirements for the SNS accelerator project. CPI performed the manufacturing optimization. AMAC as primary contractor was awarded a contract by Jefferson lab to provide three SNS prototype coupler windows using AMAC-1 window assembly design. CPI performed the fabrication. Three AMAC-1 prototypes have been high RF power tested and qualified to SNS technical specifications by Jefferson Lab. This paper mainly focuses on the design optimization, key simulation results of HFSS, MAFIA, ANSYS, electron-multipacting program results, and the mechanical design features as well. The fabrication and the cold test are described in a separate presentation in this workshop.

## 1 INTRODUCTION

The various applications of superconducting Radiofrequency (RF) Accelerators in many fields around the world have increased rapidly [1]. High power RF windows are critically important to the reliability of storage rings and linear accelerators. If a window breaks, an entire accelerator section will go from high vacuum up to air, causing a great deal of time and money in maintenance costs. High power RF couplers depend on the reliability of windows to provide the transition from air to vacuum in the RF line between the RF power sources to the accelerator cavities [2, 3, 4, 5]. The cost and complexity of RF couplers has grown dramatically in the last 10 years because of the difficulty in manufacturing these complex RF systems, and because of the mechanical, electrical, and thermal stresses the window must take during operation. At the same time, there is always the demand for RF systems that deliver higher power [6].

Under DOE's support, AMAC developed coaxial RF windows and couplers, and successfully developed, designed and prototyped a 200kW CW high RF input power waveguide type window which was high RF power tested & qualified by Jefferson Lab through a CRADA. Based on these proven qualifications, AMAC and CPI (subcontractor) were awarded a contract to produce three prototype SNS high RF input power coupler windows.

They were delivered; high RF power tested, and qualified to meet the SNS technical requirements. The SNS technical requirement are briefly listed in the following:

VSWR: 1.05 or lower at 805 MHz

Power input: 550 kW peak traveling wave

Beam on pulse length: 1.0 ms RF on pulse length: 1.3 ms Pulse repetition rate: 60 Hz RF active duty factor: 8.7%

Standing wave in full reflection: 4 MW (up to  $150 \mu s$ )

Average power: 53 kW (with 10% margin) Maximum radiative heat loss to 2.1K circuit: 1 W

Operating pressure:  $<5 \times 10^{-9}$  torr

Radiation resistance at tip of antenna:  $4 \times 10^8$  rads

During the task of prototyping three SNS prototype coupler windows, we developed several design concepts, then performed evaluation and optimization of the relative merits based upon the following RF and mechanical considerations: (1) RF properties, (2) Design maturity, (3) Thermal and mechanical design for perimeter cooling

<sup>\*</sup> This work was partly funded by a US Department of Energy SBIR grant (No DE-FG02-99-ER82739),and a contribution from CPI.

and structures, (4) Anti-multipactor design (with regards to the relative magnitude of electric fields near the window)[7, 8], and (5) Manufacturing Processes [9, 10, 11]. Results are described in the sections below. Figure 1 shows a 3-D drawing and a picture of AMAC-1 SNS high RF Input Power window.

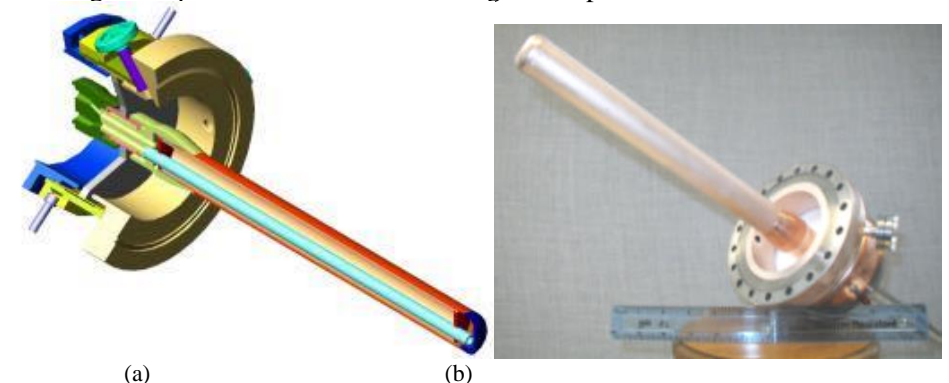


Figure 1 (a) 3D-model of AMAC-1 coupler, (b) AMAC-1 SNS coupler

# 2 AMAC-1 SNS COUPLER WINDOW DESCRIPTION

AMAC-1 is a coaxial type of coupler with a planar ceramic window separating the vacuum side from air side [12]. In the HFSS simulation, the inner and outer conductor are treated as conductor boundary with finite conductivity (5.8E+7 siemens/m). The loss tangent is taken as 0.0002, and the permittivity value is 9.6.

The SNS cryostat geometry requires a coaxial 805 MHz coupler design with a waveguide transition, and the installation of the RF ceramic window in a  $-30^{\circ}$  standing wave phase angle position. This coupler design is similar to the high power coupler successfully employed at KEK, Japan. The geometry incorporates chokes at the inner and outer conductor. Water cooling is used to remove the dissipated power at the window and the antenna.

The vacuum side of the ceramic window is coated with 10-15 Angstrom Titanium Nitride. Figure 2 shows the coupler geometry and the electric field distribution. Figure 3 shows the general window geometry.

After extensive RF calculations, using MAFIA and HFSS programs, the design was further analyzed for their multipacting behavior with a program from the University of Helsinki [2]. The calculated results also provided good comparative information for a novel design for 200kW average power operation presented in a different paper in this workshop.

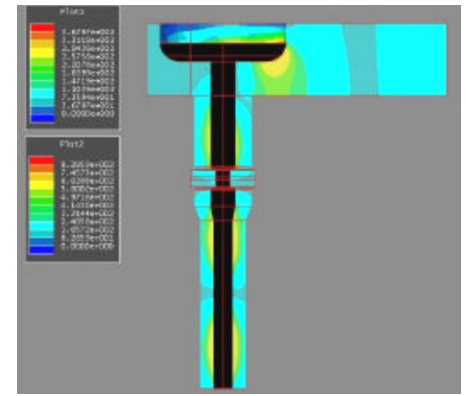


Figure 2 AMAC-1 Coupler, Electric Fields (V/m for 1W average power)

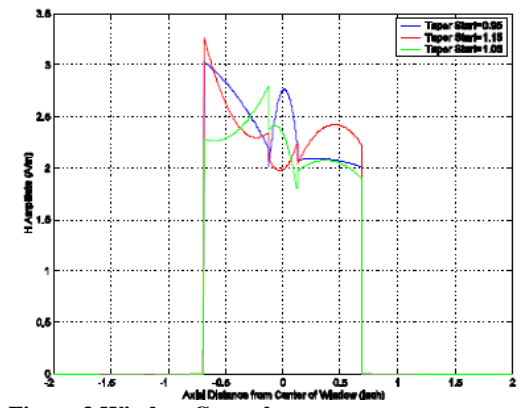


Figure 3 Window Geomelry

# 3 RF-PARAMETER OPTIMIZATION

We carried out a series of simulations using different parameters to optimize the performance of the AMAC

window. The following tables show the simulations results for 1 Watt average input power.

In the tables, PE is the peak E field along the surface of the inner conductor. The maximum electric field value occurs at the choke tip. PH means the Peak magnetic field at the joint of the ceramic window with inner conductor. P.D. ratio is the ratio of power loss at the ceramic window and the metalization layer.

Conductivity is in the unit of Siemens/m. Unless otherwise noted, the length is in unit of inch.

The line with a shaded background and a "\*" is the optimized design.

Change the start position of the taper (Fig 2.1,2.2 and 2.3):

Taper start	S11	S12	VSWR	PD ratio (E-3)	PE (V/m)	PH (A/m)
0.95	0.02858	0.99953	1.0588	0.123	1060	2.75
1.05	0.02668	0.99958	1.0548	0.1280	900	3.*
1.15	0.02565	0.99961	1.0527	0.1219	845	2.2

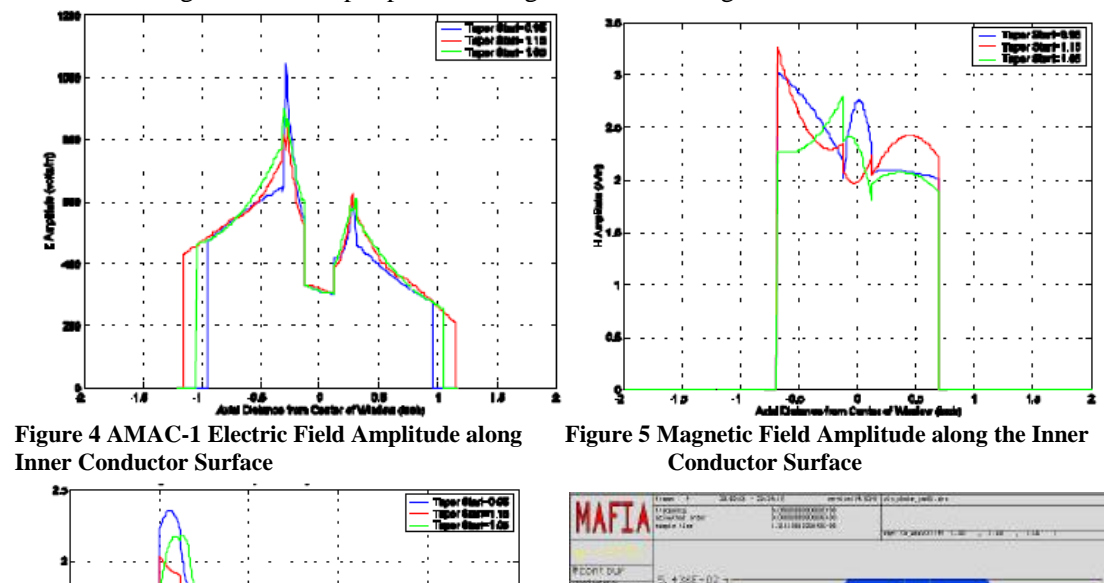
Effect of metalization (P.D. is the total loss in the ceramic and the metal layer):

Conductivity	S11	S12	VSWR	PD ratio (E-3)	PE (V/m)	PH (A/m)
0.11E-7	0.02634	0.99954	1.0541	0.2260	900	2.4*

Change the choke gap from the ceramic center plane:

change the choice gup from the certainte center plane.						
Chop gap	S11	S12	VSWR	PD ratio (E-3)	PE (V/m)	PH (A/m)
0.225	0.03448	0.99934	1.0714	0.1307	870	2.5
0.250	0.02668	0.99958	1.0548	0.1280	900	3.
0.275	0.02085	0.99972	1.0426	0.1252	820	2.4*

Figures 4, 5 and 6 show the results of the HFSS calculations for the E and H field distribution for the standard AMAC window design for 1KW input power. In Figs 4 and 5, the negative side is the air side of the window.



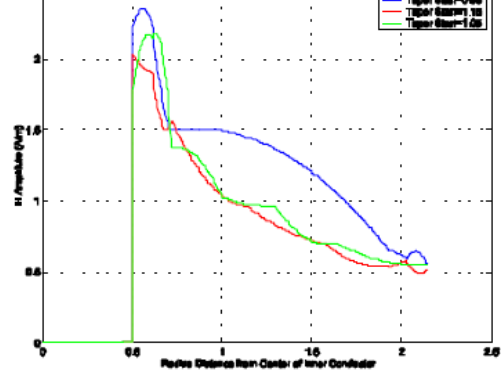


Figure 6 Magnetic Field Amplitude along the

### 100 | 100 | 100 | 100 | 100 | 100 | 100 | 100 | 100 | 100 | 100 | 100 | 100 | 100 | 100 | 100 | 100 | 100 | 100 | 100 | 100 | 100 | 100 | 100 | 100 | 100 | 100 | 100 | 100 | 100 | 100 | 100 | 100 | 100 | 100 | 100 | 100 | 100 | 100 | 100 | 100 | 100 | 100 | 100 | 100 | 100 | 100 | 100 | 100 | 100 | 100 | 100 | 100 | 100 | 100 | 100 | 100 | 100 | 100 | 100 | 100 | 100 | 100 | 100 | 100 | 100 | 100 | 100 | 100 | 100 | 100 | 100 | 100 | 100 | 100 | 100 | 100 | 100 | 100 | 100 | 100 | 100 | 100 | 100 | 100 | 100 | 100 | 100 | 100 | 100 | 100 | 100 | 100 | 100 | 100 | 100 | 100 | 100 | 100 | 100 | 100 | 100 | 100 | 100 | 100 | 100 | 100 | 100 | 100 | 100 | 100 | 100 | 100 | 100 | 100 | 100 | 100 | 100 | 100 | 100 | 100 | 100 | 100 | 100 | 100 | 100 | 100 | 100 | 100 | 100 | 100 | 100 | 100 | 100 | 100 | 100 | 100 | 100 | 100 | 100 | 100 | 100 | 100 | 100 | 100 | 100 | 100 | 100 | 100 | 100 | 100 | 100 | 100 | 100 | 100 | 100 | 100 | 100 | 100 | 100 | 100 | 100 | 100 | 100 | 100 | 100 | 100 | 100 | 100 | 100 | 100 | 100 | 100 | 100 | 100 | 100 | 100 | 100 | 100 | 100 | 100 | 100 | 100 | 100 | 100 | 100 | 100 | 100 | 100 | 100 | 100 | 100 | 100 | 100 | 100 | 100 | 100 | 100 | 100 | 100 | 100 | 100 | 100 | 100 | 100 | 100 | 100 | 100 | 100 | 100 | 100 | 100 | 100 | 100 | 100 | 100 | 100 | 100 | 100 | 100 | 100 | 100 | 100 | 100 | 100 | 100 | 100 | 100 | 100 | 100 | 100 | 100 | 100 | 100 | 100 | 100 | 100 | 100 | 100 | 100 | 100 | 100 | 100 | 100 | 100 | 100 | 100 | 100 | 100 | 100 | 100 | 100 | 100 | 100 | 100 | 100 | 100 | 100 | 100 | 100 | 100 | 100 | 100 | 100 | 100 | 100 | 100 | 100 | 100 | 100 | 100 | 100 | 100 | 100 | 100 | 100 | 100 | 100 | 100 | 100 | 100 | 100 | 100 | 100 | 100 | 100 | 100 | 100 | 100 | 100 | 100 | 100 | 100 | 100 | 100 | 100 | 100 | 100 | 100 | 100 | 100 | 100 | 100 | 100 | 100 | 100 | 100 | 100 | 100 | 100 | 100 | 100 | 100 | 100 | 100 | 100 | 100 | 100 | 100 | 100 | 100 | 100 | 100 | 100 | 100 | 100 | 100 | 100 | 100 | 100 | 100 | 100 | 100 | 100 | 100 | 100 | 100 | 100 | 100 | 100 | 10

Figure 7 Contour plot of magnetic field in AMAC-1 at

#### Ceramic Window Surface

## 1/2W incident power

Figures 7 and 8 show the MAFIA calculation results for the electric and magnetic fields for 0.5 W incident power. Figure 9 is a contour plot of the dielectric loss in the ceramic. Figures 10(a) and 10(b) show the dielectric loss distribution, and the electric fields at the center plane of the ceramic for 1W incident power.

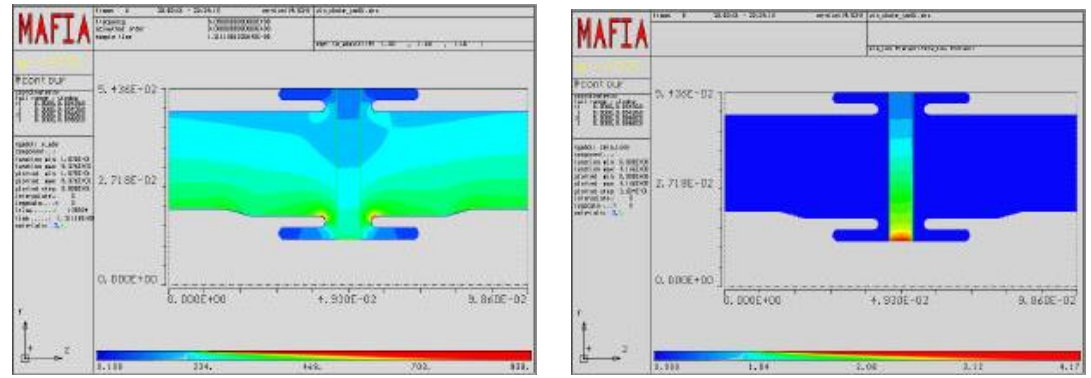


Figure 8 Contour plot of electric field in AMAC-1 Figure 9 Contour plot of AMAC-1 dielectric losses in at 1/2W incident power the ceramic at 1/2W incident power

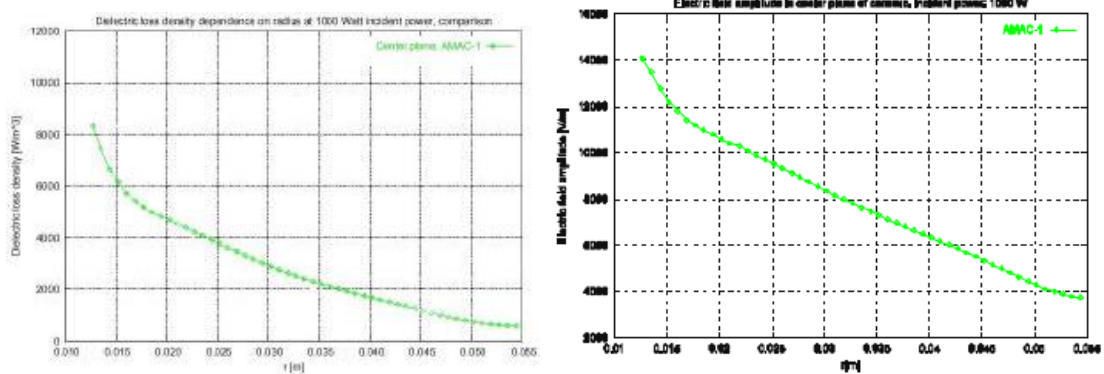


Figure 10a Radius dependence of dielectric loss at Figure 10b Radius dependence of electric field at the 1000W incident power for AMAC-1 ceramic center plane of AMAC-1 at 1000 W of incident power

## 3.1 Tolerance Analysis

To study the tolerance of the RF coupler to manufacture errors, we varied some important dimensions and properties and recalculated the Voltage Standing Wave Ratio (VSWR) and Power Dissipation Ratio.

# 3.2 Summary of RF Calculations

Window Assembly only, 53 kW average Power: S11: 0.00864 S12: 0.99939 VSWR: 1.0174 Power Loss in the Ceramic: 6.5 W (LT=0.0002) Power Loss at the Copper Surface: 54 W

Peak Electric Field: 27.5 kV/m (at the choke corner)

Peak Magnetic Field: 91.4×10<sup>-6</sup> Tesla (at the ceramic inner boundary)

Insertion Loss: -0.0053 dB

## 4 THERMAL AND STRESS CALCULATIONS

The caluculations were done using the ANSYS finite element program. Figures 11 to 13 show some of the results. According to the stress calculations, the highest tensile stress in the ceramic window is around 2.1 ksi, which is admissible to the tensile strength of Alumina used in the design. It was also found that asymmetric

cooling at the inner and outer side of the ceramic window will result in rise of the highest tensile stress in ceramic window.

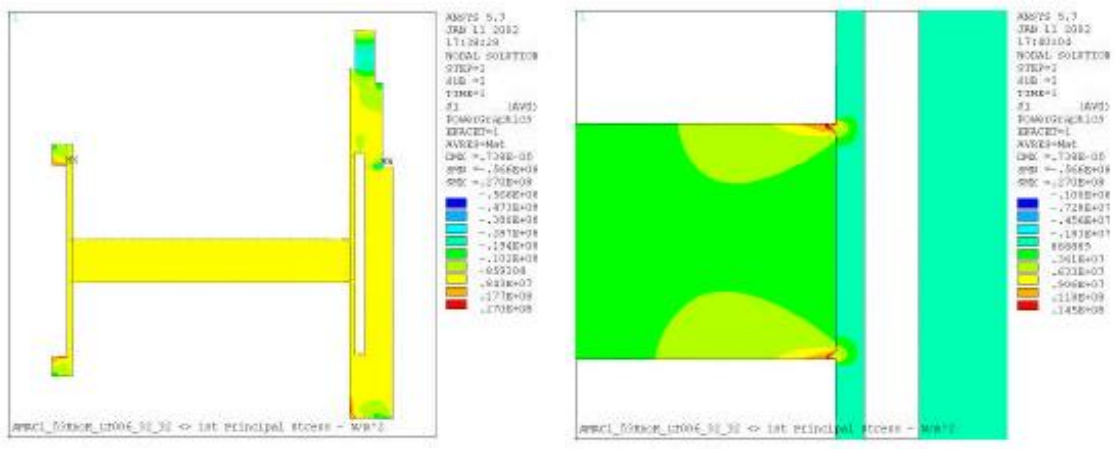


Figure 11 1st principal stress distribution

Figure 12 Maximum 1st principal stress in ceramic

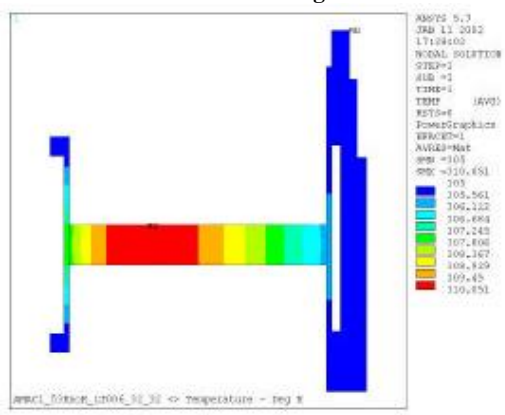
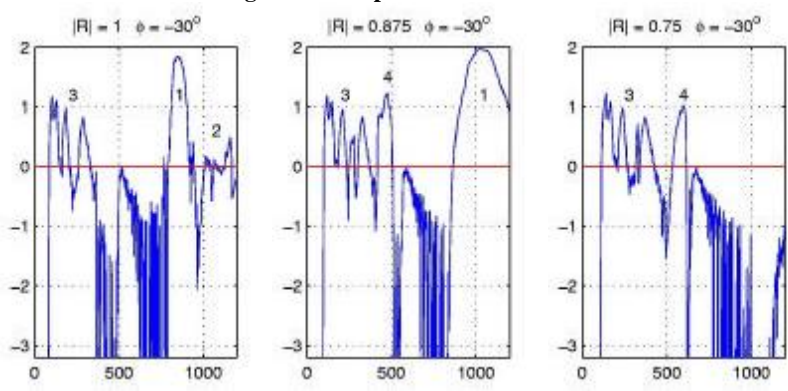
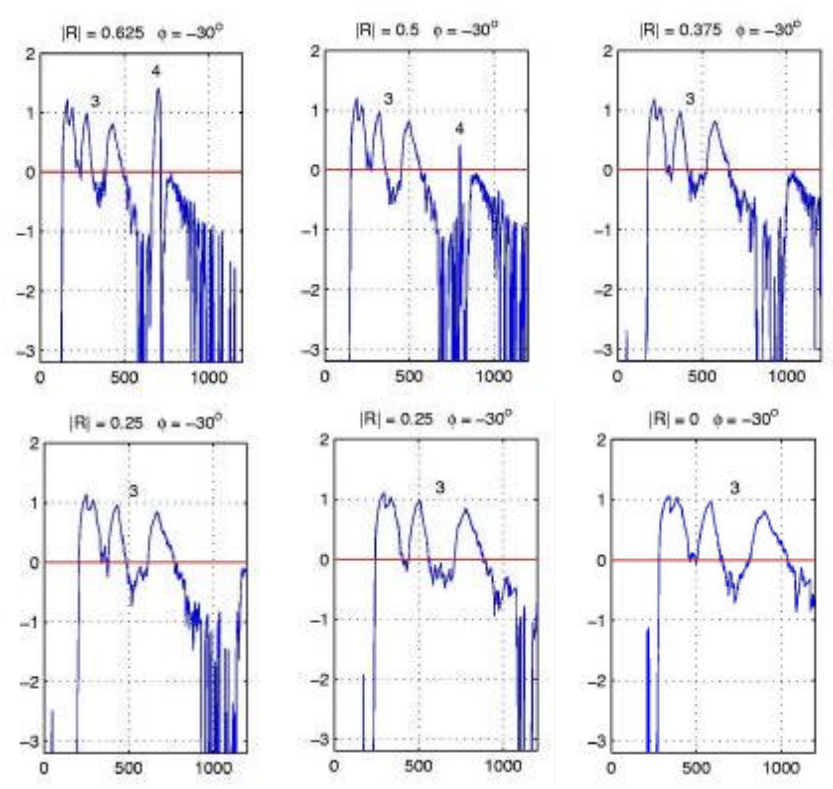


Figure 13 Temperature distribution





**Figure 14 Relative Enhanced Counter Function** 

#### 5 MULTIPACTING CALCULATION RESULTS

Secondary electron emission data for copper extended to 50eV on the lower energy side was used in the calculations for all copper and copper plated surfaces. The secondary electron emission values for TiN were used for the ceramic window surface.

The calculations were performed at the University of Helsinki [3] under a subcontract from AMAC with a specially developed program which tracks electron trajectories in various wave reflection conditions and determines their enhancement possibility for different power levels.

These calculations are considered a reliable indication of multipacting occurring due to secondary electron emission on the coupler surfaces in the vacuum region, and are used to validate the coupler geometry in the design stage.

The description and results of the calculations are shown in Figs. 14 and 15. R=1 corresponds to full reflection (standing wave) with an electric minimum at the center of the window, and R=0 corresponds to a traveling wave condition. The SNS window is installed at a phase position of –30 degrees.

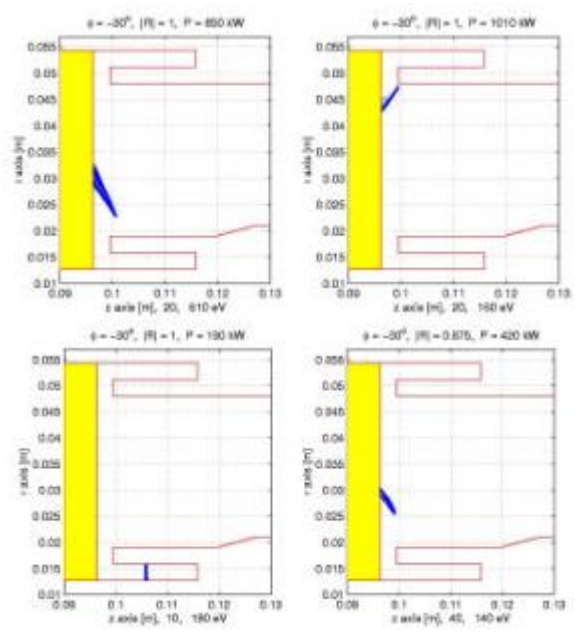


Figure 15 Electron trajectories

## **6 RF TEST RESULTS**

The coupler windows have been conditioned and successfully RF tested at the Jefferson Laboratory to meet the SNS specifications [3]. Figure 16 shows the high RF power test fixture of AMAC-1 SNS coupler.



Figure 16 Jefferson Lab Test Stand with two AMAC-1 windows

## 6.1 Preparation procedure (pressure rinse, bakeout, ultimate vacuum, RGA, etc.).

After receiving the window assemblies, incoming inspection of the windows was performed (visual, mechanical measurements, vacuum leak checks, cleaning conform JLAB procedure for admission in a clean room class 100, assemble the vacuum side of the couplers (outer conductors, window assemblies and associated instrumentation – optical view ports for arc detectors, vacuum gauges and electron pick up antennae on a connecting waveguide). The connected waveguide with the vacuum side of the coupler assembled was transferred and connected to the vacuum group of the test cart, pumped down and vacuum leak checked, prepared for baking, baked, assembled the water cooling pipes, check for water leak, assembled the air side of the coupler, perform low RF power measurements, inserted in the waveguide structure and RF processed. Vacuum leak check was performed using the RGA on the test cart. The same RGA instrumentation was used to monitor molecular species during baking and RF processing. Baking was done using the JLAB baking system (heater, temperature sensors, snaps switch protections, and computer controls) and procedure (ramping temperature up with 10

Celsius degree per hour, soaking for 24 hours at 200 C then ramping down at room temperature with 10 Celsius degrees per hour). While baking version A2 at 200 C a snap or a glitch in the program has trigger power on heaters OFF for about 15 minutes. The baking process has been recovered after resetting the program. Vacuum at the end of baking was better than 10-9 mbar.

6.2 RF conditioning on the test stand (Vacuum response vs. power and pulse length, and vacuum residual gas analysis).

Conditioning and testing at room temperature was performed at JLAB using the 1 MW RF system consisting of a klystron, waveguide distribution system, terminating load or variable short circuit, directional couplers and associated RF power meters, electronic racks for klystron controls, coupler instrumentations, interlocks, software for RF processing and data acquisition. Coupler No1 was on the klystron side, coupler No2 on the RF terminating load (Short circuit). The process consisted in starting conditioning in TW mode with low RF power amplitude and duty cycle and increasing the RF power amplitude and duty cycle to the specifications (our capabilities were limited by RF system to 1 MW, 6% duty cycle. After reaching maximum RF power, the RF was cycled between different power levels, or maintained constant for an extended period of time (similar with machine operation). During conditioning and high power RF testing, vacuum, electron activity, arcing events, temperatures and flows on the cooling water, and RGA were continuously recorded.

6.3 Conditioning times.

In TW mode, the time to reach 1 MW (1 ms, 30 Hz at the end) was about 24 hour of RF conditioning. 6.4 Water temperature rise, flow rate and pressure drop at maximum RF power.

The flow was maintained constant at about 0.3 gpm (actually it was at the control limit of out valves), antenna and the border of the ceramic windows being "cooled" in series by the same water circuit on the same coupler. No T change on temperature readings (under our measurement conditions) or water flow were identify during long term constant power tests on both versions of window. Temperatures at the windows were always about 32 Celsius degrees (temperature of the cooling water)

6.5 Electron activity

Electron activity (about 20 nA) started to manifest during long constant RF power test (525 kW, pulse duration 1.15 ms, repetition 60 Hz). This long constant power test was performed for 24 hours, approaching nonstop conditions of operation in the machine (1.3 ms, 60 Hz, 550 kW), split in two portions of 12 hours each. In the first run, random, sporadic vacuum and electron activity have started after about 3 hours of tests. In the consecutive run, this pattern was almost continuous –from the beginning of the test. There is a dependence of the magnitude of the electron activity on pulse characteristics (pulse length, repetition rate).

No bias voltage was applied during all these tests.

6.6 Power RF results (power, vacuum and other limitations or results)

The AMAC-1 coupler has been tested in TW mode and in SW mode:

- In TW mode up to 1 MW (1 ms, 30 Hz), test "CW" at 1 MW for about 60 minutes O.K.
- In TW mode,  $2 \times 12$  hours constant power test at 550 kW (1.15 ms, 60 Hz) spurious vacuum and electron Activity.
- In SW mode up to 2.8 MW local peak power (pulse duration 0.15 ms, repetition rate 60 Hz).

# 7 ACKNOWLEDGMENTS

We wish to thank Genfa Wu, and Lulin Yuan for the RF analysis and calculations, and the Jefferson Lab IFSCS for the preparation and testing of the couplers.

## 8 REFERENCES

- [1] Q. S. Shu, "Large Applications and Challenges of state of the art Superconducting RF (SRF) Technologies," Advances in Cryogenic Engineering. Plenum: New York, NY, 1997.
- [2] D. Proch, ed. (DESY), "Superconducting RF Input Coupler Workshop," Hamburg, 1998.
- [3] B. Dwersteg (DESY), "Progress of the TTF High Power Input Coupler Design at DESY," Proceedings of the 8th RF Superconductivity workshop, Abano Terme, Italy, 1997.
- [4] S. Mitsunobu (KEK), "High Power Input Coupler and Windows," Proceedings of the 8<sup>th</sup> RF Superconductivity workshop, Abano Terme, Italy, 1997.

- [5] M. Neubauer, M. Allen, K. Fant, A. Hill, M. Hoyt, J. Judkins, H. Schwarz (SLAC), R.A. Rimmer (LBL, Berkeley). "High Power Testing off PEP-II RF Cavity Windows," SLAC-PUB-7209, Jun 1996. 4pp. Talk given at 5th European Particle Accelerator Conference (EPAC 96), Sitges, Spain, 10-14 Jun 1996. Published in EPAC 96:2059-2061.
- [6] S. Chel, et. al. (Saclay/Orsay), "Coaxial Disc Windows for a High Power Superconducting Cavity Input Coupler," Preceedings of the 1999 Particle Accelerator Conference, New York, 1999.
- [7] Humphries, S., "Electron Multipactor Code for High-Power RF Window Development," Particle Accelerators, 1998.
- [8] Chel et. al., "Coaxial Disc Windows for a High Power Superconducting Cavity Input Coupler," PAC New York, 1999.
- [9] Schmierer, et. al., "Development of the SCRF Power Coupler for the APT Accelerator," proc of PAC, New York, 1999.
- [10] Mitsunobu, et. al., "High Power Input Coupler for the KEKB SC Cavity."
- [11] Kindermann, et. al., "RF Power Tests of LEP2 Main Couplers on a Single Cell Superconducting Cavity." CERN-SL-97-64.
- [12] Q. S. Shu, "Technical Report on SBIR Phase I and Phase II," Supported by US DOE Grant No. DE-FG02-99-ER82739, AMAC International, Inc., 2002.